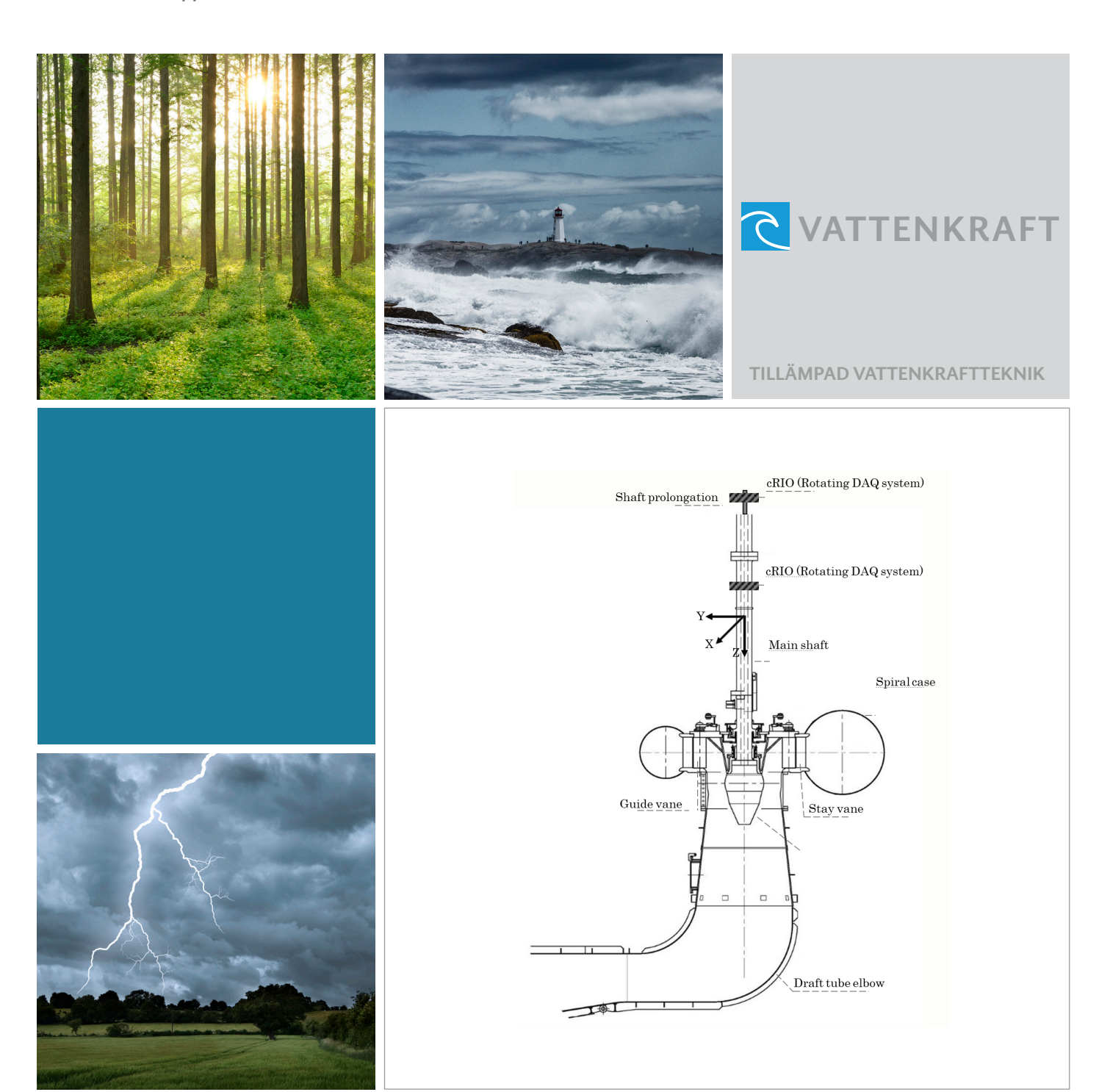
LOADS ON KAPLAN RUNNER DURING STEADY OPERATIONS

REPORT 2021:776





Loads on Kaplan runner during steady operations

Investigation of the coupling between the blades and shaft

ARASH SOLTANI DEHKHARQANI MICHEL CERVANTES

Foreword

The role of hydropower is changing from being a base load provider to a load balancing power to enable a greater influx of intermittent energy sources to the system. This reflects itself in changing operational patterns for hydropower and an increase in off-design operation, suspected to greatly shorten the technical life span of the machinery. It is of great importance to further the understanding and knowledge in this area.

This project, Loads on Kaplan runner during steady operations, by Arash Soltani Dehkharqani provides the industry with more easily available methods to assess the loads on turbines from off-design operation and is an important piece in trying to understand the costs associated with providing balancing power. It was developed through a cooperation between The Swedish Hydropower Centre (Svenskt vattenkraftcentrum) and the Energiforsk programme Applied hydropower technology (Tillämpad Vattenkraftteknik).

These are the results and conclusions of a project, which is part of a research programme run by Energiforsk. The author/authors are responsible for the content.



Summary

Hydropower plays a major role in the energy market by providing approximately 60% of renewable electricity. The penetration of intermittent energy sources, such as solar and wind power, seriously influences the energy balance as well as the stability of the electrical grid. Therefore, the smooth integration of this share into the existing power grids is highly demanded. Hydraulic power plants are one of the key components to stabilize the electric grid. As a result, the off-design operation of hydraulic turbines increases, and hydraulic turbines are subject to unstable flow conditions and unfavorable load fluctuations. Predicting load fluctuation on the runner using indirect measurements can provide an optimized operating range for the turbine unit, increase turbine refurbishment time intervals, and avoid structural failures in extreme cases.

This project aims to investigate an experimental methodology to assess and predict the flow condition and loads on a Kaplan turbine runner by performing strain measurements on the shaft. An experimental measurement campaign was performed on a full-scale Kaplan turbine, Porjus U9. In the measurement campaign, several operational conditions ranging from start-up, speed-no-load, steady-state, load variations, emergency shutdown, runaway, and stop were examined. Steady-state and load variation measurements were carried out under on-cam and off-cam conditions, i.e., mimicking the operation of a propeller. Miniature pressure transducers and strain gauges were installed on a runner blade. Axial, bending, and torsion measurements were performed on the turbine shaft. The results show that for any propeller curve of a Kaplan turbine, the guide vane opening corresponding to the minimum pressure and strain fluctuation on the runner blade can be obtained by the axial, torsion, and bending measurements on the shaft. Torsion measurements on the shaft could support index-testing in Kaplan turbines. Furthermore, a signature of every phenomenon observed on the runner blade signals, e.g., runner frequency, rotating vortex rope, and rotor-stator interaction, is found in the data obtained on the shaft. Fatigue analysis shows that part-load operating conditions may cause more fatigue compared to start/stop.

Keywords

Hydropower, turbines, part-load, Kaplan, Porjus U9, speed-no-load, steady-state. Vattenkraft, turbiner, dellast, reglering, flexibilitet.



List of content

1	Intro	duction	6
2	Expe	rimental Setup	9
	2.1	Porjus U9 prototype	9
	2.2	Instrumentation	9
		2.2.1 Blade surface preparation and wiring	11
		2.2.2 Pressure measurement on the runner	13
		2.2.3 Strain gauge measurement on the runner	14
		2.2.4 Strain gauge measurement on the shaft	15
		2.2.5 Turbine general parameters measurement	16
	2.3	Measurement program	17
3	Data	Analysis	19
	3.1	Time-average	19
	3.2	Spectral analysis (steady-state measurement)	19
	3.3	Peak-to-peak value	20
	3.4	Fatigue Analysis	20
4	Resul	lts	21
5	Conc	lusion	31
6	Refer	rences	32



1 Introduction

Renewable energies provided 26.2% of the global electricity generation and reached 2378 GW in capacity in 2018, see Figure 1.1 [1]. Hydropower plays an important role among the renewable energy sources and provides approximately 60% of the renewable electricity accounted for 4210 TWh in 2018 [1].

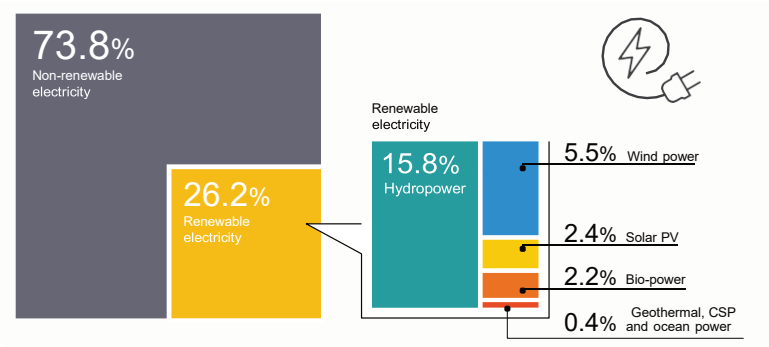


Figure 1.1: Estimated renewable energy share of global electricity production. Reproduced from [1]

There is a growing trend in the capacity of installed renewable energy sources (not including hydropower) in 2008-2018 [1]. This is along with the energy policies concerning the reduction of greenhouse gas emissions, which led to promoting the development of alternative renewable energy sources such as solar and wind power. Similar to the global trend, electricity production using renewable sources increased in Sweden and reached approximately 58% in 2017 [2]. Hydropower was the largest source of energy production that accounted for 65 TWh, more than nuclear power electricity generation, see Figure 1.2.

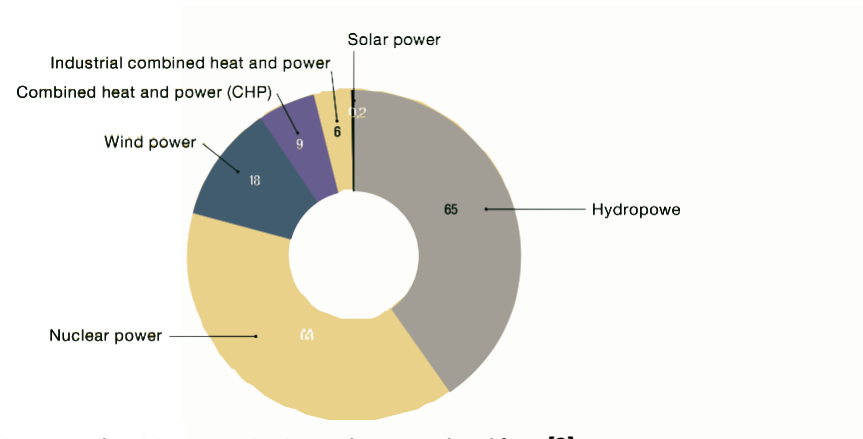


Figure 1.2: Electricity generation in Sweden. Reproduced from [2]

Off-design operations of hydraulic turbines, ranging from turbine start-up to full load and turbine shut-down, involve considerable complexity in the flow such as flow separation and vortex breakdown. The undesirable flow phenomena induce load fluctuations on the runner blades which can affect the structural and rotodynamic behavior of the turbine. Nevertheless, hydraulic turbines are



designed to operate at a certain operating point for a specific head and discharge, known as the best efficiency point (BEP). Rotor-stator interaction (RSI), rotating vortex rope (RVR), guide vane wakes, flow separation on the runner, vortex breakdown, hub vortices, and tip vortices are examples of phenomena resulting in periodic excitation forces [3-6]. The effects of transients, load fluctuations, and the flow interaction on the hydraulic turbine's runner were reviewed in [7-9]. Not only fatigue-related problems such as wear and tear on the turbine components but vibration issues also may arise from the load fluctuations which can result in severe failures [10-13]. The performance and lifetime of the turbine bearings can be significantly influenced by the periodic and random load fluctuations [14, 15].

In 2016, a research group at the Polytechnic University of Catalonia in collaboration with university and industrial partners performed a measurement campaign on a prototype medium-head Francis turbine located in British Columbia, Canada. This turbine has a rated power of 444 MW and a runner diameter of 5.4 m. It was aimed to propose an optimized strategy for field tests regarding the best suitable sensor locations on the turbine rotating and stationary components [16]. Unit instrumentation consisted of different transducers; pressure transducers and strain gauges installed on the runner blades, pressure transducers installed on the draft tube cone, spiral case, and penstock, torsion strain measurement on the shaft, proximity sensors for the shaft displacement, as well as accelerometers in the turbine bearings, draft tube wall, and spiral casing wall. Different turbine operations were investigated, and different phenomena such as vortex rope, cavitation, runner mechanical resonance, and hydraulic resonance were detected. However, any correlation between the shaft and runner blade measurement was not reported. Part load operation and load variation in two prototype Francis turbines (one vertical and one horizontal) were experimentally investigated by pressure measurement at the draft tube wall [17]. Higher pressure fluctuations were observed at the part-load operation compared to the BEP operation. In the same measurement campaign, the pressure fluctuations during the load increase from 50% to 70% were 1.6 times larger than the one obtained during steady-state operation at 50% load [18]. A measurement on a 200 MW prototype Francis turbine showed that shaft oscillations increased at part load operation when the pressure fluctuations were intense in the draft tube [19]. Different start- up sequences were examined on a prototype propeller turbine by performing strain measurements on a runner blade [20]. Although the maximum strain on the runner blade did not decrease at the optimized start-up sequence, the strain fluctuations decreased at the beginning of the cycle. Gagnon et al. [21] demonstrated that reducing the guide vane opening rate can reduce the crack propagation rate on the runner blades of a prototype Francis turbine. Jansson [22] performed strain measurements on the shaft of the Porjus U9 prototype Kaplan turbine during the turbine start-up. A wide-band frequency at low-frequency region (around 0-5 Hz) with high intensity occurred prior to synchronous speed.

Prototype turbine measurements are prohibitively expensive and time-consuming, this explains the small number of literatures on the subject. Unfortunately, reduced scale turbine model measurements do not predict all characteristics of prototype turbines. For example, the synchronous component of the vortex rope can be considerably damped or amplified depending on the hydraulic system [23, 24].



This lack of similarity necessitates the experimental investigation of prototype hydraulic turbines during design and off-design operations for the safe and long operation of hydraulic turbines. Therefore, simple measurement methodologies, e.g., measurements on the shaft, for prototype machines to predict the flow characteristics and the impact of the operating conditions on the runner structure are needed, the object of this study.

The primary goal of this project is to investigate the interaction of the flow and turbine runner blades as well as the shaft on a Kaplan prototype, Porjus U9, during different operating conditions. To achieve this goal, a measurement campaign has been performed to investigate several operational conditions ranging from startup, speed-no-load, steady-state, load variation, runaway, emergency shutdown, and shutdown. Pressure and strain fluctuations on a runner blade and shaft were investigated.



2 Experimental Setup

This section describes the experimental setup including the turbine specifications, data acquisition system, and installed transducers together with a description of the operating conditions. Note that only part of the information that is related to this project is presented. Detailed information can be found in [23].

2.1 PORJUS U9 PROTOTYPE

Experimental measurements have been carried out on a full-scale Kaplan turbine, Porjus U9. This turbine, located along the Lule river, Sweden, is part of the Porjus Hydropower Center and is primarily used for research and educational purposes. The turbine is composed of 6 runner blades, 20 equally spaced guide vanes, and 18 unequally distributed stay vanes with a runner diameter of 1.55 m. The runner is located approximately 7 m below the tailwater. The penstock has a total length of approximately 67.1 m with three elbows. The diameter of the penstock varies between 10.5 m at the penstock inlet and 2 m before the spiral case inlet. The draft tube length is approximately 11 m. Table 2.1 presents the nominal operating parameters of this turbine.

Table 2.1 Nominal operating parameters of the Porjus U9 prototype Kaplan turbine

Parameter	Value	Unit
Head (H)	55.5	[m]
Power (P)	10	[MW]
Discharge (Q)	20	$[m^3s^{-1}]$
Rotational speed (n)	600	[RPM]

2.2 INSTRUMENTATION

Different types of transducers have been installed on the rotating and stationary components of the prototype turbine; pressure transducers and strain gauges on an individual runner blade, strain gauges on the turbine shaft, accelerometers in the runner cone, proximity transducers close to the runner guide bearing, and an optical encoder to measure the turbine rotational speed. Note that accelerometers and proximity transducers are not considered in this report. A unique data acquisition system has been designed and employed to collect and store the data.

The analog signals from the transducers have been collected by a data acquisition system composed of two rotating and one stationary slave chassis and one master computer. Each slave had an NI cRIO-9014 embedded real-time controller. The signals from the rotating slave chassis have been transmitted to a wireless network connected to the master computer. One of the rotating slave chassis has been installed on the top of the turbine shaft where the pressure transducers and strain gauges on the runner blade have been connected to this unit. A NI 9205 module and five NI 9237 modules have been installed on this unit. The NI 9205 (±10 *VV*, 16-bit) has been configured for differential measurement and therefore 16 channels have been available. Each NI 9237 module had four channels with 24 bits resolution. An excitation of 5 V has been used for each NI 9237. A small slip ring



was used to power the rotating slave chassis. The other rotating slave chassis has been installed on the shaft between the generator guide bearing and turbine guide bearing to digitize the signals from the strain gauges installed on the shaft. It consisted of two NI 9237 modules. The shaft has been instrumented with a slip ring to power the rotating slave chassis. The stationary slave chassis has acquired the turbine operational parameters such as guide vanes opening, runner blades opening angle, power output, headwater level, tailwater level from the turbine control room. The signals from the distance transducers, installed near the turbine guide bearing to acquire the shaft displacement, and an optical encoder have been also digitized by the same unit. The signals have been oversampled at 5 kHz to avoid any aliasing and then digitally downsampled to 2.5 kHz. Figure 2.1 and Figure 2.2 present the location and view of two rotating slave chassis installed on the shaft and top of it.

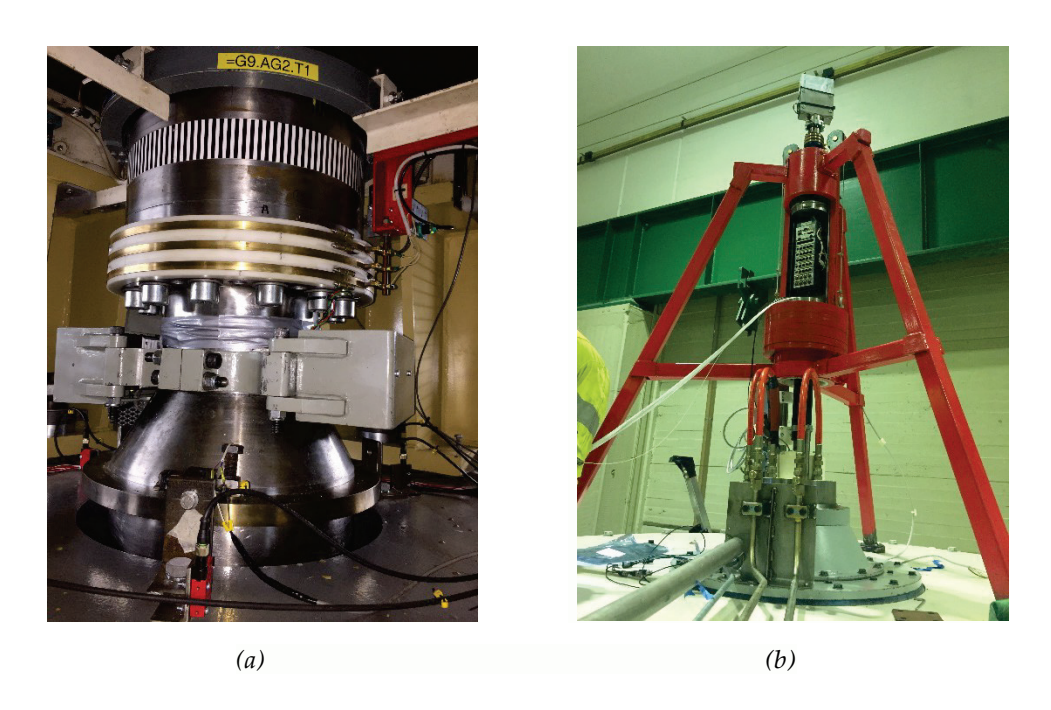


Figure 2.1: The rotating slave chassis installed (a) on the turbine shaft, (b) on top of the shaft.



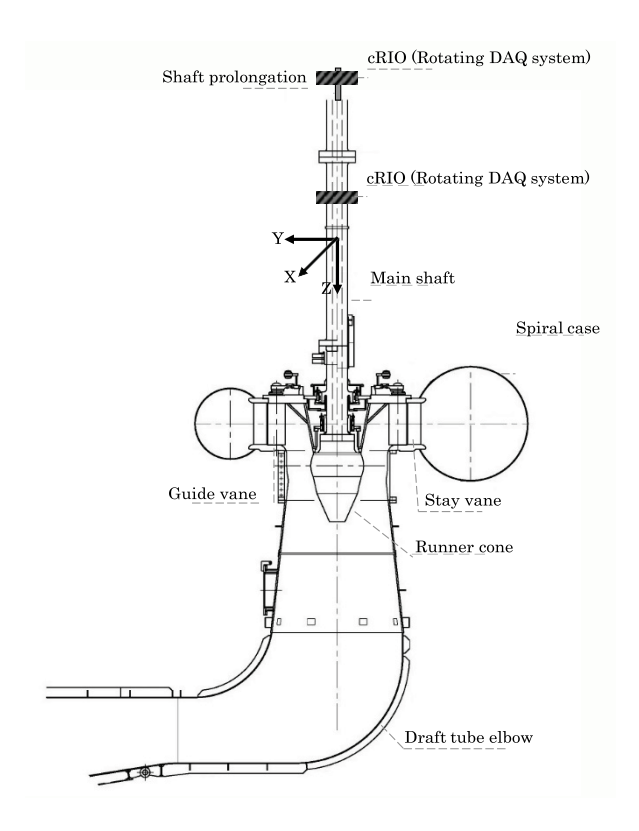


Figure 2.2: Schematic of the Porjus U9 prototype Kaplan turbine and the location of the rotating slave chassis.

2.2.1 Blade surface preparation and wiring

Proper surface preparation is an essential prerequisite for adhesive bonding. Prior to blade instrumentation, two runner blades with a 180° spacing were sandblasted. One blade was chosen for instrumentation and the other one used to avoid hydraulic and mass imbalance resulted from the weight of the applied epoxy on the instrumented blade. Two different types of epoxies were applied on the runner blade. Two-component Belzona 1311 was applied on the blade as the base epoxy and two-component Belzona 1341 was used as the anti-cavitation coating. Table 2.2 presents the characteristics of the applied epoxies to the runner blade.

The high strength base epoxy was used due to the high shear and normal forces on the blade. The anti-cavitating agent was applied to the base epoxy, when the base layer was cured, to decrease the roughness of the surface. However, the local pressure disturbances generated by the epoxy surface roughness was unavoidable. Finally, an equal amount of epoxy applied to the target blade was applied to the other blade to achieve hydraulic and mass balance. Figure 2.3 shows a view of two runner blades.



Table 2.2 The specification of applied epoxies to the runner blade.

	Parameter	Value	Unit
Belzona 1311	Mixing ratio by weight (Base : Solidifier)	5:1	-
	Mixed density	2.36-2.52	$[g/cm^3]$
	Tension shear (applied to stainless steel)	19	[MPa]
	Compressive strength	56.8	[MPa]
Belzona 1341	Mixing ratio by weight (Base : Solidifier)	100 : 70	-
	Mixed density	1.42	$[g/cm^3]$
	Tension shear	24.8	[MPa]
	Compressive strength	57.2	[MPa]





Figure 2.3: The prepared runner blades (a) the suction side of the blade which is used to achieve hydraulic andmass balance, (b) the suction side of the instrumented blade with pressure transducers and strain gauges. The hydraulic hose mounted to protect the electrical cable is visible on the right of each picture.

Kaplan turbine runner blades are adjustable during the turbine operation, with a considerable movement during the turbine start-up. One of the main challenges in this instrumentation was to have variable cable lengths to take into account the blade rotation and protect the cables from the high fluid velocity. All the cables followed the blade surface, passed over the blade at the leading edge, and reached the blade suction side close to the hub. Then, the cables were guided through a hydraulic hose to enter the runner cone. Thereafter, all the cables passed through the hollow shaft and reached the top of the generator. Figure 2.4 shows the hydraulic hose and its installed location on the turbine. The insulated cable of $4 \times \text{UBA3219 TAU}$ manufactured by Industrifil was used. The linear resistance of this cable was $0.5 \ \text{Ohm/m}$.





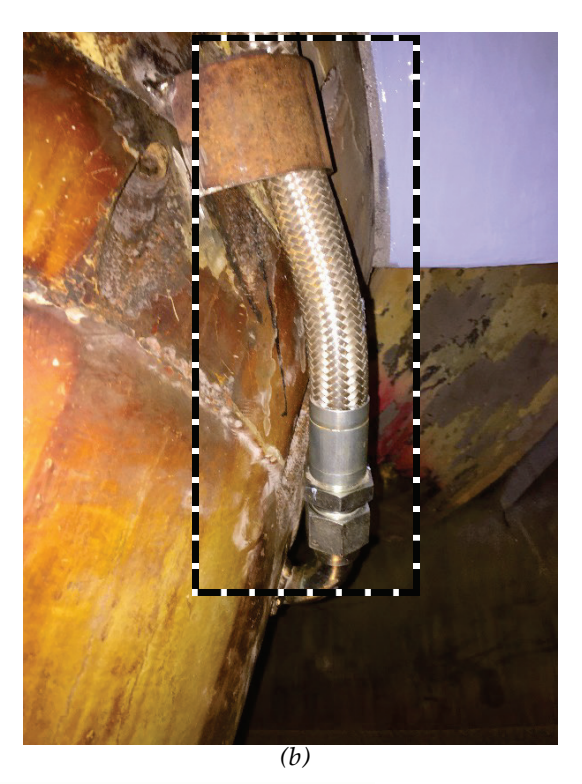


Figure 2.4: The hydraulic hose to guide the cables from the blade surface to the runner cone and hollow shaft (a)one end of the hydraulic hose attached to the runner blade hub, (b) the other end of the hydraulic hose attached to the runner cone.

2.2.2 Pressure measurement on the runner

Transient pressure measurements were performed on a runner blade pressure and suction side. The piezo-resistive pressure transducers were encapsulated to be easily installed on the blade and isolate the transducers and their connection from the applied epoxy. Twelve miniature pressure transducers manufactured by Kulite (LL-080 series) were used. The operating range of the pressure transducers is 0-700 kPa, and their natural frequency is 380 kHz. Six pressure transducers were installed on the pressure side (P-PS-1 to P-PS-6) and six of them on the suction side (P-SS-1 to P-SS-6) of one runner blade. The first letter of the transducer name stands for the quantity measured, i.e., the pressure P. The second part describes the location of the measurements, e.g., the blade pressure side (PS) or suction side (SS). The numbering begins with the transducer installed near the leading edge and tip and proceeds to the one close to the trailing edge hub. The transducers were installed on the intersection of imaginary circles that pass through 1/3 and 2/3 of the blade's span and 1/4, 1/2, and 3/4 of the blade's chord lines. The locations were obtained from the pressure measurement performed by Amiri [24] on the corresponding U9 Kaplan model. Eight pressure transducers were connected to the NI 9237 module and four other pressure transducers were connected to the NI 9205 module. Figure 2.5 shows the position of the pressure transducers on the runner blade pressure side.



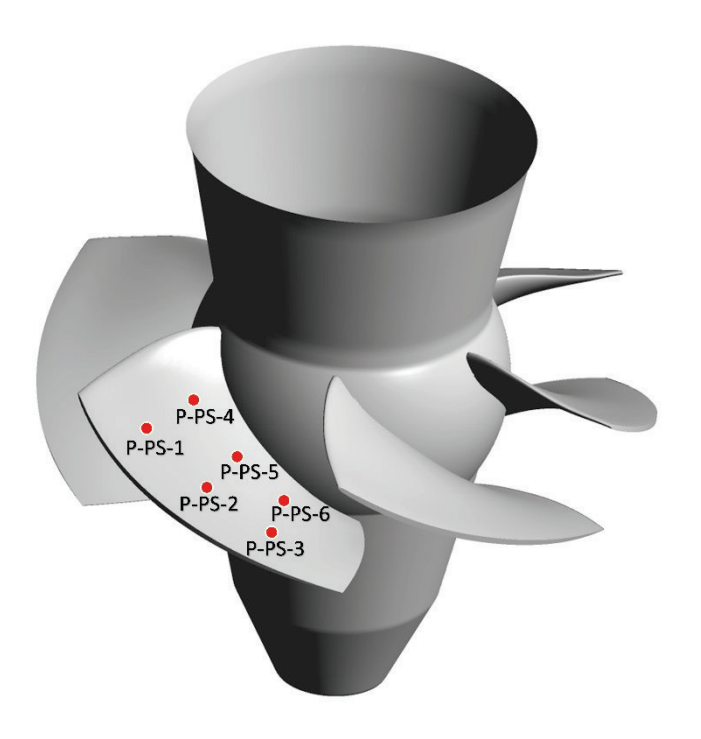


Figure 2.5: Position of the pressure transducers on the runner pressure side [REF].

2.2.3 Strain gauge measurement on the runner

Following a preliminary one-way fluid-structure coupled simulation and modal analysis, three points on the runner blade were spotted to install the strain gauges; one near the leading edge, one close to the runner blade hub, and a third point close to the trailing edge. The region close to the runner blade hub is generally subjected to high stress. Higher structural deflection can be observed near the blade trailing edge. Two uniaxial strain gauges (K-LY41- 6/350-3-2M manufactures by HBM) were installed at each point in the tangential and radial direction on the blade pressure and suction side, respectively. Therefore, twelve uniaxial strain gauges were installed on the runner blade. The resistance and gauge factor of the strain gauges were $350 \pm 0.35\%$ and $2.07 \pm 1\%$, respectively. Figure 2.6 shows the position and arrangement of the strain gauges on the runner blade pressure side. The strain gauges were named similar to the pressure transducer. The first letter stands for the measurement quantity, i.e., strain. The second part describes the location of the measurements, e.g., the blade pressure side (PS) or suction side (SS). The numbering begins with the transducer installed near the blade leading edge on the pressure side and proceeds to the one close to the trailing edge on the suction side. The last letter stands for the direction of the strain gauge, e.g., the radial direction (R) or tangential direction (T). The transducer S-PS-2R corresponds to the strain gauge located on the pressure side at point 2 close to the blade hub in the radial direction. Material expansion due to surrounding flow temperature is compensated in the selected strain gauges. The strain gauges were calibrated onsite using the shunt calibration technique.



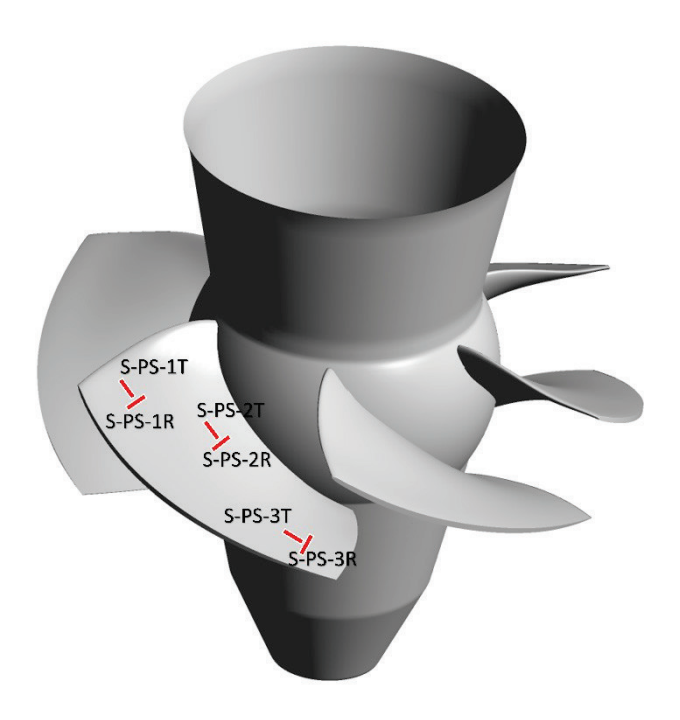


Figure 2.6: Position and arrangement of the strain gauges on the runner pressure side [ref]

2.2.4 Strain gauge measurement on the shaft

Axial strain, bending strain in two directions, and torsional strain were obtained using six strain gauges installed on the turbine shaft surface between the generator guide bearing and turbine guide bearing. Four uniaxial strain gauges, the same type used for the strain measurement on the blade, were installed in the axis direction with a 90° spacing to measure the axial strain and bending strain in two directions. The shaft torsional strain measurement was performed using two torsion strain gauges (K-XY41-6/350-3-2M manufactures by HBM) installed on the same shaft section in the axis direction with a 180° spacing. The resistance and gauge factor of the torsional strain gauges were 350 \pm 0.35% and 2.08 \pm 1%, respectively. Figure 2.7 presents the arrangement of the axial and torsion strain gauges on the shaft.



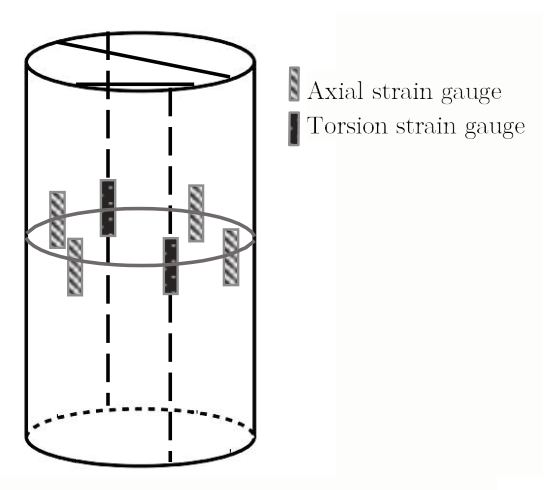


Figure 2.7: The arrangement of the strain gauges on the turbine shaft

2.2.5 Turbine general parameters measurement

As earlier mentioned, all the provided turbine operational parameters from the turbine control system (e.g., guide vane opening, runner blade opening angle, power output, headwater level, and tailwater level) were simultaneously obtained. In addition, the guide vane opening was measured by a distance transducer of wire type installed on the guide vane hydraulic servomotor to acquire the linear movement of the guide vanes. Figure 2.8 shows the distance transducer mounted on the servomotor. The runner blade angle and the guide vane angular opening range of this unit is +10° to -17° and 0-35° (0-100% opening), respectively. An optical encoder was installed close to the shaft to measure the turbine rotational speed. The accuracy of the optical encoder was 3°.

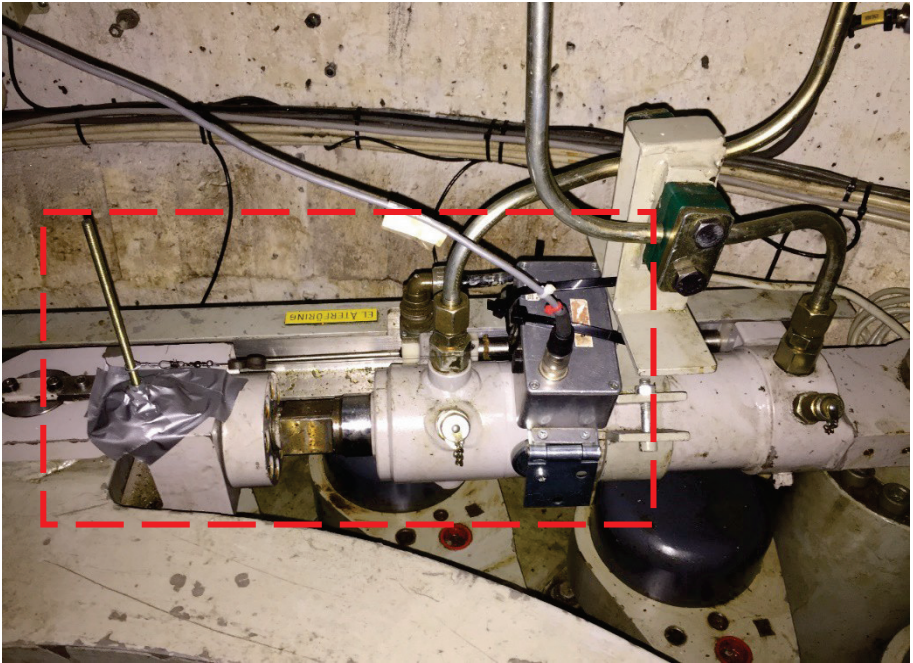


Figure 2.8: Distance transducer to measure the guide vane opening.



2.3 MEASUREMENT PROGRAM

The experimental investigation of the turbine has been performed at several operational conditions and comprised start-up, speed-no-load, steady-state, load variation, emergency shutdown, runaway, and shutdown. The steady-state and load variation measurements have been carried out under on-cam and off-cam conditions. During the on-cam operation, the runner blade angle is automatically adjusted by the governor according to the predefined hill chart determined from an index test. However, the blade angle is set to a prescribed angle and held constant during the off-cam operation and the turbine is operated as a propeller turbine. Three guide vane openings have been selected under the on-cam condition called OP1, OP2, and OP3. For the load variation operations, the guide vane opening was changed from one steady point to another. The guide vane opening rate was controlled by the governor. Six possible load variations between the steady-state operating points have been performed. In addition, two propeller curves have been used to investigate the off-cam operation; runner blade angle of +3.9° (OP4-OP8) and -4.3° (OP9-OP13). All possible load variations between the operating points of each off-cam condition have been investigated except for the load variations that involved OP5 and OP7 in the first off-cam operation and OP10 and OP12 in the second off-cam operation. Table 2.3 presents the specification of the investigated operating conditions during the measurement campaign.

Table 2.3 Specification of the investigated operating conditions

Operating point	GV opening [%]	Runner blade angle [⁰]	
OP1	43	-13.5	
OP2	63	-4.3	On-cam operation
OP3	83	+3.9	
OP4	66	+3.9	
OP5	74	+3.9	
OP6	83	+3.9	First off-cam operation
OP7	91	+3.9	
OP8	98	+3.9	
OP9	44.5	-4.3	
OP10	55.6	-4.3	
OP11	64	-4.3	Second off-cam operatio
OP12	72	-4.3	
OP13	80	-4.3	
OP14	15	-13.5	Speed-no-load condition
OP15	From 0	-7	Start-up
OP16	From 30.2	From -17.11	Runaway condition
OP17	From 49.2	From -9.9	
OP18	From 15.7	From -17.1	Emergency shutdown
OP19	From 63	From -4.3	
OP20	From 91	From +3.9	Shutdown
OP21	From 72	From -4.3	



The measurements have been started with the on-cam operation and proceeded with the first and second off-cam operations. Thereafter, the performed measurements have been repeated once. Thus, each steady-state and load variation have been repeated at least four times to ensure the repeatability of the measurements and obtain a statistically representative result. Nevertheless, it was very difficult to repeat an exact operating point in this machine as the governor was adjusting the runner blade angle and guide vane opening. Finally, the speed-no-load, runaway, and emergency shutdown conditions have been carried out. Shutdown operation has been performed during the on-cam and off-cam measurements.



3 Data Analysis

3.1 TIME-AVERAGE

Averaging of the acquired pressure and strain data during steady-state and load variation is carried out using MATLAB Savitzky–Golay filter smoothing filter. A polynomial order of two and a window size of 5 s are used after a sensitivity analysis. The signal fluctuating component is obtained by subtracting the time-averaged value from the original signal.

(3.1)

$$\tilde{X}(t) = X(t) - \bar{X}(t)$$

where \tilde{X} is the fluctuating component, X is the instantaneous value, X is the time-

averaged value obtained with the Savitzky–Golay filter smoothing filter, and t is the time. The fluctuating component is used for spectral analysis. The arithmetic mean of time-averaged value is determined for the steady-state data. Figure 3.1 presents the normalized pressure data obtained from the P-PS-2 during a load increase. The white line indicates the time- averaged value. The pressure data is normalized with respect to the initial pressure value in the turbine chamber before running the measurement (P_{ref}). However, absolute strain values are reported.

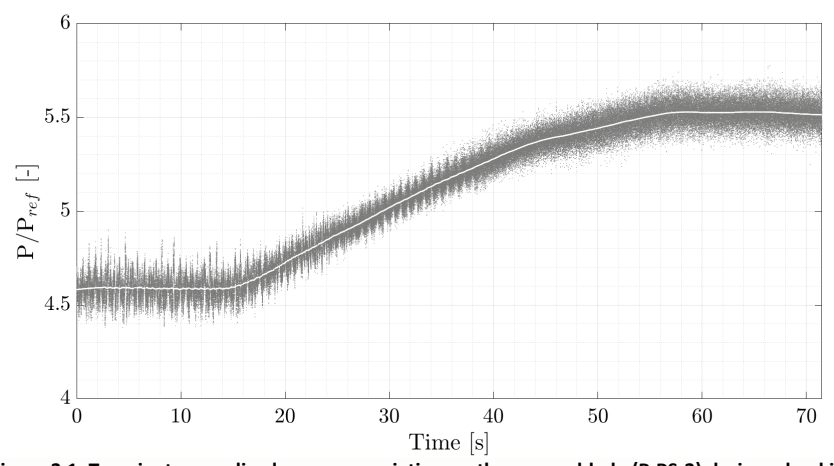


Figure 3.1: Transient normalized pressure variation on the runner blade (P-PS-2) during a load increase; gray dots: instantaneous data; white line: time-averaged data.

3.2 SPECTRAL ANALYSIS (STEADY-STATE MEASUREMENT)

The spectral analysis of the steady-state data is carried out to determine the dominant frequencies of the flow. Welch's method with a Hanning window is



applied to the fluctuating component of the pressure and strain data. The steadystate data is divided into six segments and an overlap of 50% is considered between the segments. The frequencies are normalized as

$$f_n = \frac{f}{N} \tag{3.2}$$

where f is the frequency component and N is the rotational frequency of the runner.

3.3 PEAK-TO-PEAK VALUE

The standard deviation is a tool to quantify the dispersion of data. The time-averaged peak-to-peak value is calculated by considering $2\sigma\sigma$, which holds approximately 95% of the highest peak of the data within the sliding window, to investigate the fluctuating amplitude of the pressure and strain data during the steady-state and load variations. A sliding window size of 0.1 s is chosen.

3.4 FATIGUE ANALYSIS

Fatigue damage analysis can provide valuable information regarding the turbine components' lifetime which is based on strain gauge measurements on turbine different components, e.g. runner blade, shaft, and bearings. Fatigue damage is accumulated in materials by the cyclic application of loads. The first step of the analysis is to split the complex measured strain data into discrete events of loading cycles. Rainflow counting method was used. The fatigue life is estimated by the damage accumulation law (Miner's rule).

$$\sum_{i=1}^{k} \frac{n_i}{N_i} = C$$

where C defines the cumulative damage. n_i and N_i are the number of counted of cycles and the number of cycles necessary to produce failure at the stress level of σ_i , respectively. N_i can be taken from the S.N curve of the material. According to the theory, when the value C = 1, failure should occur.

The S.N curves of the blade and shaft material were provided. Therefore, a comparative method is introduced as follow:

$$\sum_{i=1}^{k} \frac{m_i}{M_i} = D$$

where D is the relative damage factor, m_ℓ is the number of counted cycles, and M_ℓ is the number of cycles at the strain level of σ_ℓ for BEP of an individual propeller curve. Therefore, the number of strain levels (bin numbers in the histogram data) for each operating point and corresponding BEP must be identical. The start-up, speed-no-load, excitation, and shutdown operation data were normalized by the BEP of the second propeller curve. Please note that this relative method is different than the Miner's rule (damage accumulation law) and could not be compared with.



4 Results

As previously mentioned in section 2.3, various operating conditions have been investigated during the measurement campaign. Figure 4.1 presents a schematic and guide vane opening of the investigated operating conditions. OP3 and OP8, specified in Figure 4.1 (b) are considered the best efficiency points for the off-cam 1 and 2, respectively.

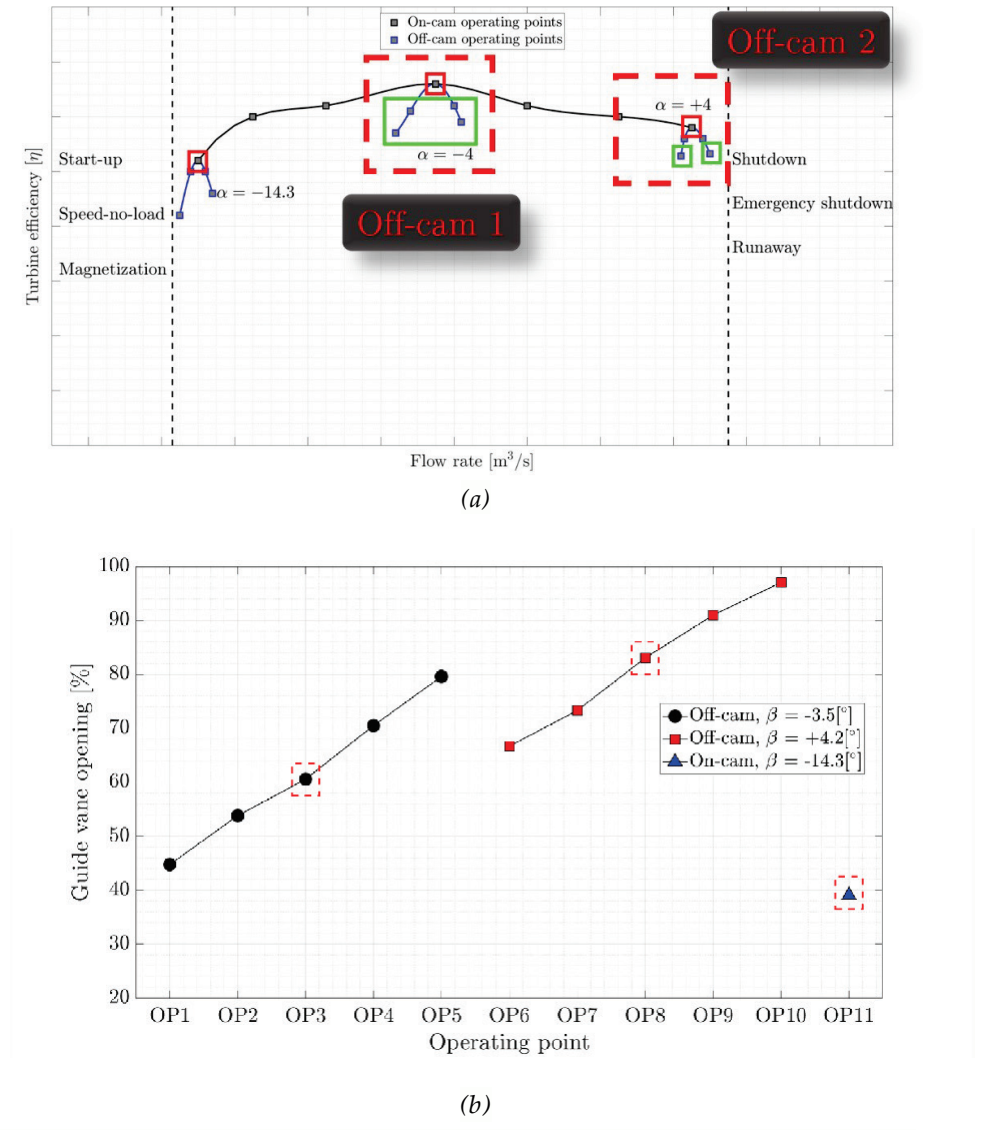


Figure 4.1: (a) Schematic of the investigated operating conditions, (b) the guide vane opening and runner blade anglevariation at the investigated operating points.

The normalized average pressure variation on the runner blade pressure side for OP1-OP11 is presented in Figure 4.2. The pressure increases for all the pressure transducers for OP1 to OP5 which can be explained by the higher flow rate due to guide vane opening. The pressure transducer located at the leading edge close to



the runner hub shows an identical behavior. However, the pressure value of the other pressure transducers decreases from OP6 to OP8 and then increases.

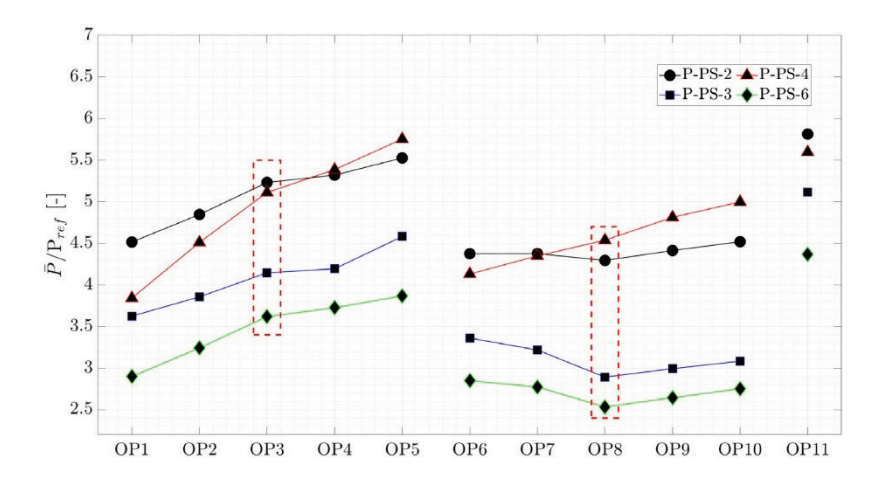


Figure 4.2: Normalized average pressure of four pressure transducers on the runner blade at OP1-OP11.

The average axial, torsion and bending strain obtained on the shaft for different operating points are presented in Figure 4.3, Figure 4.4, and Figure 4.5, respectively. As expected, the axial and torsion strain increase with the guide vanes opening for each propeller curve, meaning from OP1 to OP5 and OP6 to OP10. Similarly, the bending strain value in the X and Y directions increases with the guide vanes opening except for the bending strain in the X direction at OP5 and bending strain in the Y- direction at OP9 and OP10. The reason for this behavior is not clear.

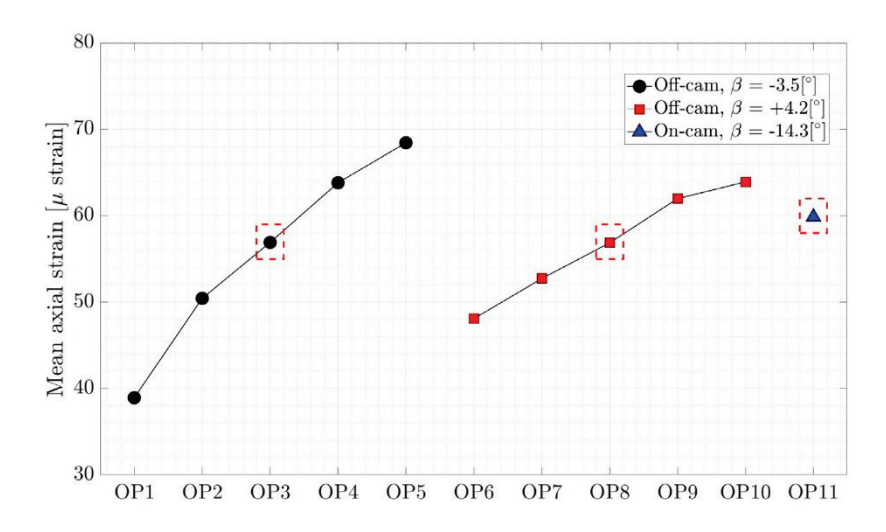


Figure 4.3: Average axial strain on the shaft at OP1-OP11.



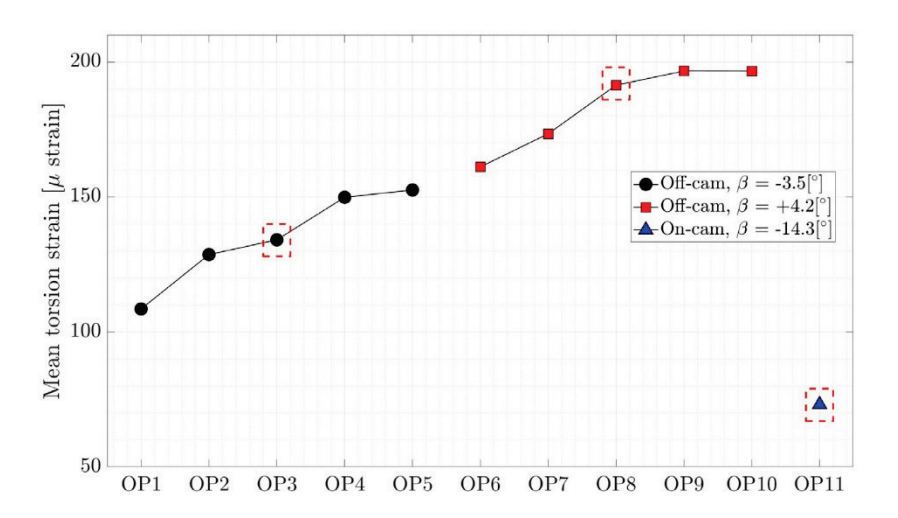


Figure 4.4: Average torsion strain on the shaft at OP1-OP11.

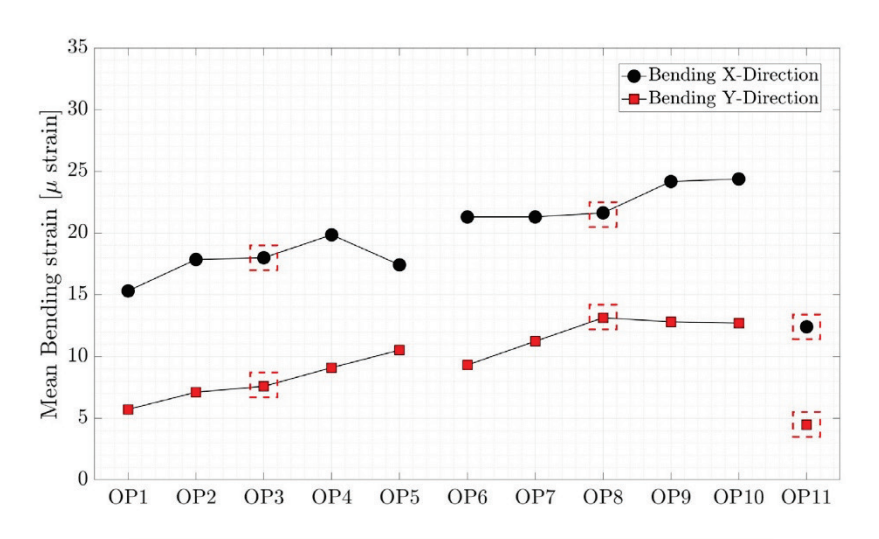


Figure 4.5: Average bending strain on the shaft at OP1-OP11.

Figure 4.6 presents the normalized pressure peak-to-peak value obtained on the runner blade at different steady-state operating conditions. The trend of the peak-to-peak variation for two propeller curves is different. In the first propeller curve, OP1-OP5, the peak-to-peak variation is rather symmetric with respect to the BEP. However, in the second propeller curve, large pressure peak-to-peak values are observed at OP6 and OP7 compared to OP9 and OP10, indicated the presence of large pressure pulsation arising from the RVR at the second propeller curve. Figure 4.7 shows the strain peak-to-peak value obtained on the runner blade at four locations. The minimum pressure and strain fluctuations of each propeller curve correspond to the BEP of that propeller curve.



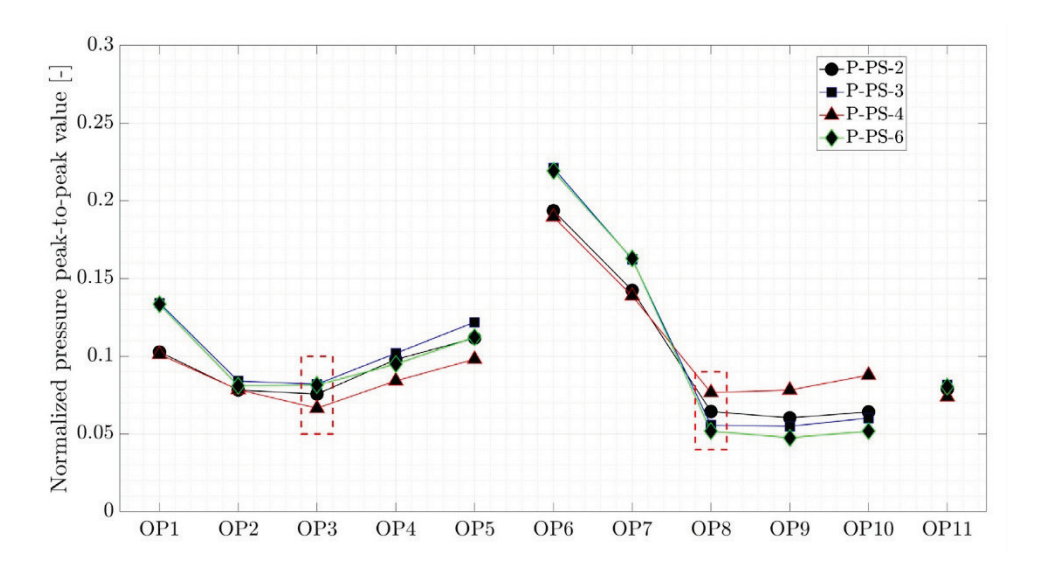


Figure 4.6: Normalized pressure peak-to-peak value of four pressure transducers on the runner blade at OP1-OP11.

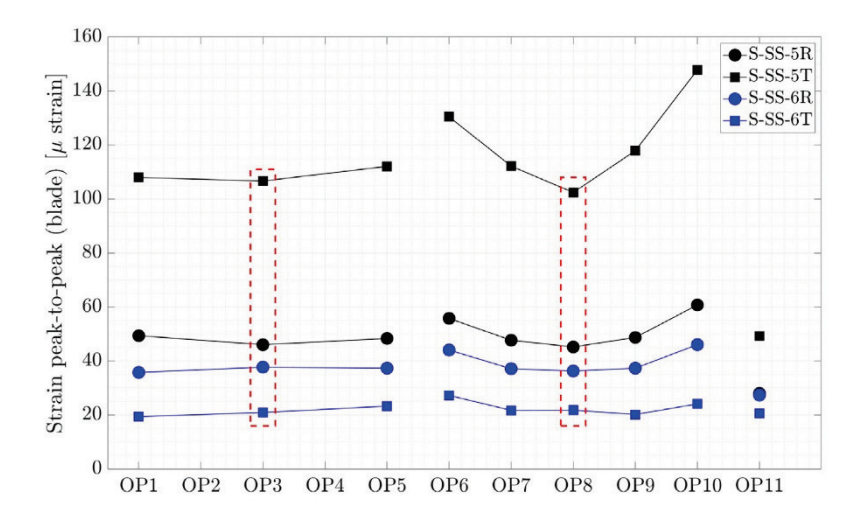


Figure 4.7: Peak-to-peak value of strain fluctuations on the runner blade at OP1-OP11.

Figure 4.8, Figure 4.9, and Figure 4.10 show the axial, torsion, and bending strain peak-to-peak value at different operating points, respectively. One can find two local minimum points in each figure occurring at OP3 and OP8. This result shows that the operating points that have minimum strain peak-to-peak values on the shaft and blade are identical.



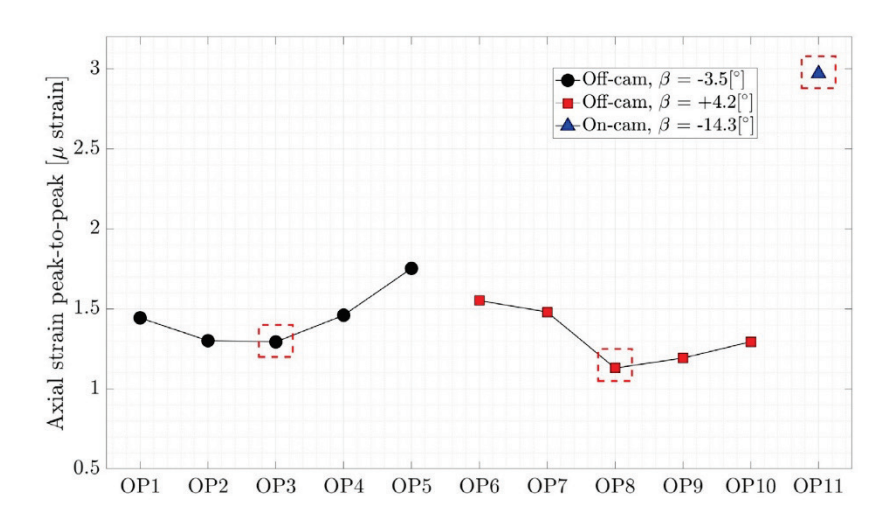


Figure 4.8: Peak-to-peak value of axial strain fluctuations on the shaft at OP1-OP11.

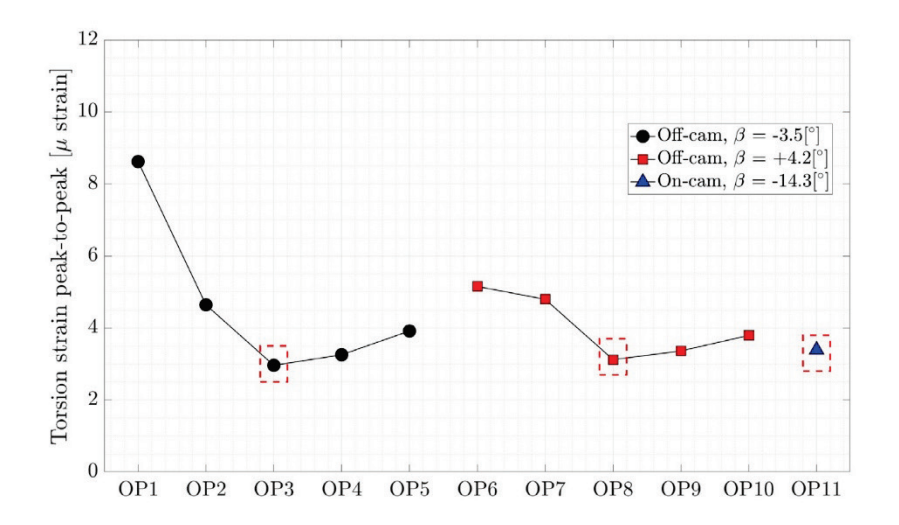


Figure 4.9: Peak-to-peak value of torsion strain fluctuations on the shaft at OP1-OP11.

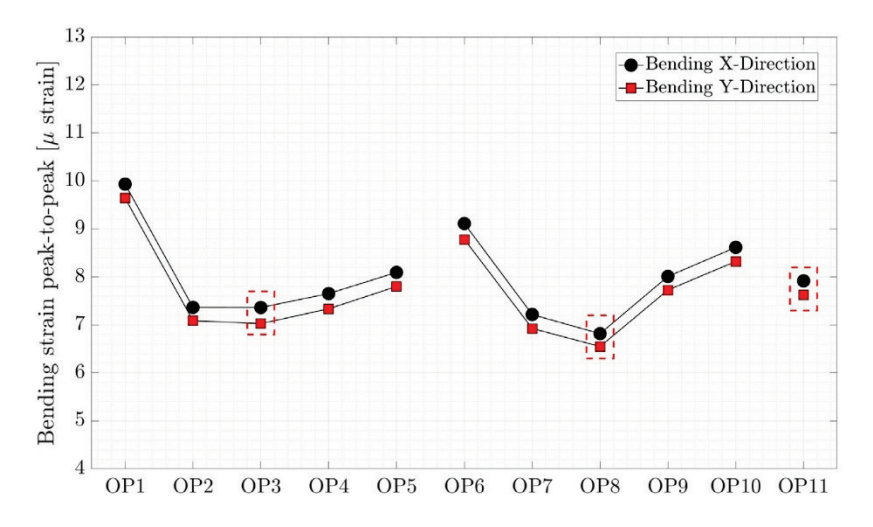


Figure 4.10: Peak-to-peak value of bending strain fluctuations on the shaft at OP1-OP11.



As previously mentioned, the main purpose of this project is to find a possible relation between the measurements on the shaft and the runner blade. The strain and pressure data obtained on the runner blade and shaft are plotted in Figure 4.11. The data for each propeller curve is normalized by the corresponding BEP value, meaning OP3 and OP8 for the first and second propeller curves, respectively. Only the pressure data of P-PS-4 and bending strain in the X-direction are plotted representing pressure data on the runner blade and bending strain on the shaft, respectively. Different behavior is observed for each propeller curve.

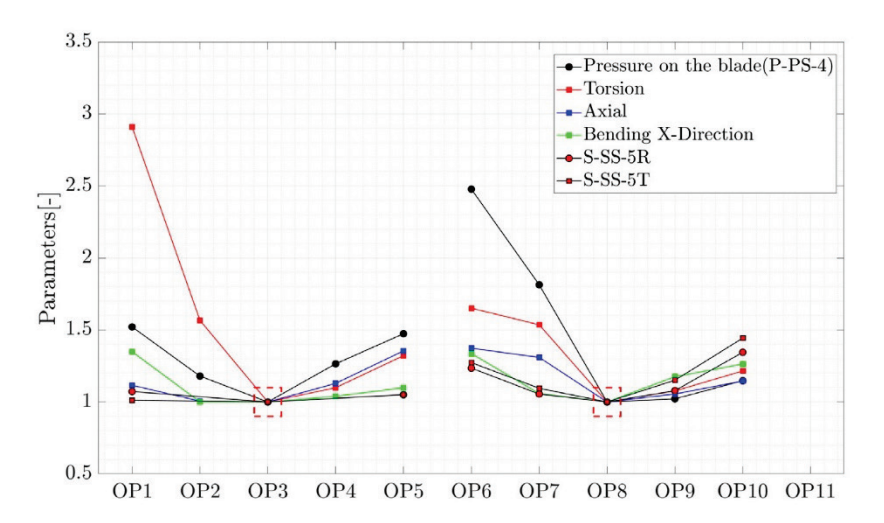


Figure 4.11: Strain and pressure data peak-to-peak values obtained on the blade and shaft normalized by the corresponding BEP data of each propeller curve.

Although any clear correlation between the blade and shaft measurement is not obtained, torsion measurements on the shaft showed that it can be used for indextesting on Kaplan turbines. Figure 4.12 presents the variation of the inverse of the torsion peak-to-peak value obtained on the shaft as a function of turbine output power. A hypothetical line, specified by the green color in the figure, can represent the cam curve. The operating points specified with the red dashed squares are assumed to be the BEP of the propeller curves.



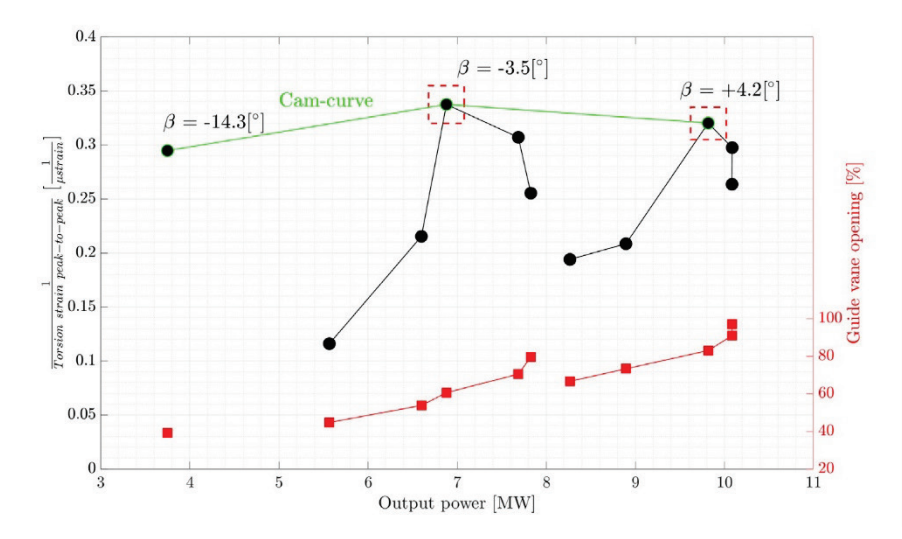


Figure 4.12: Inverse of torsion peak-to-peak value obtained on the shaft as a function of turbine output power. Red dots correspond to guide vane opening. The green line is a hypothetical cam curve.

Spectral analysis of the data obtained on the runner blade and shaft at different steady-state operating conditions was performed. Figure 4.13 presents the waterfall plots of three operating points chosen from a propeller curve where the flow rate increases from OP1 to OP5. The rotating vortex rope, plunging mode ($f_n = 0.15 \sim 0.18$) and rotating mode ($f_n = 0.82 \sim 0.85$), are clearly observed in Figure 4.13 (a) and (b) for different transducers. The plunging mode is seen in the pressure data as well as axial and torsion strain obtained from the shaft. The rotating mode is observed in most of the data including pressure, strain gauge in the radial direction, torsion, and bending strain. By increasing the flow rate at OP2, similar results are observed in the frequency spectrum with the plunging mode appearing in the strain data obtained on the blade. By further increasing the flow rate at OP5, the vortex rope frequencies disappear and only the runner frequency $(f_n = 1)$ and its second harmonic remain in the frequency spectrum (low-frequency region). The frequency spectrum of the same operating points in the highfrequency region is presented in Figure 4.14. Guide vane passing frequency ($f_n = 20$) is observed in the pressure and strain data obtained on the blade. However, it is only detected in the axial strain measurements on the shaft. This proves that a signature of every phenomenon observed in the data obtained on the runner can also be seen in the data on the shaft.



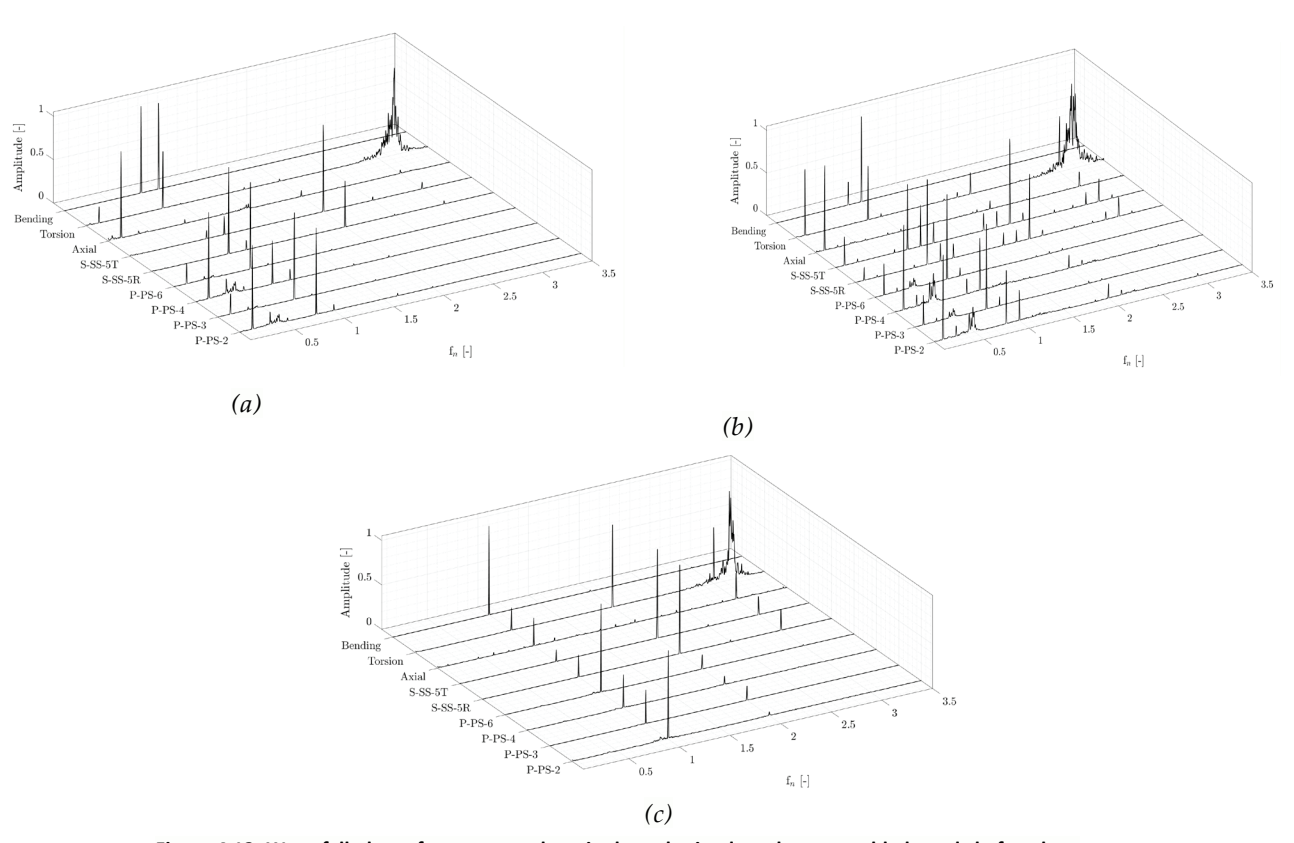


Figure 4.13: Waterfall plots of pressure and strain data obtained on the runner blade and shaft at low-frequency region; (a)OP1, (b) OP3, and (c) OP5.

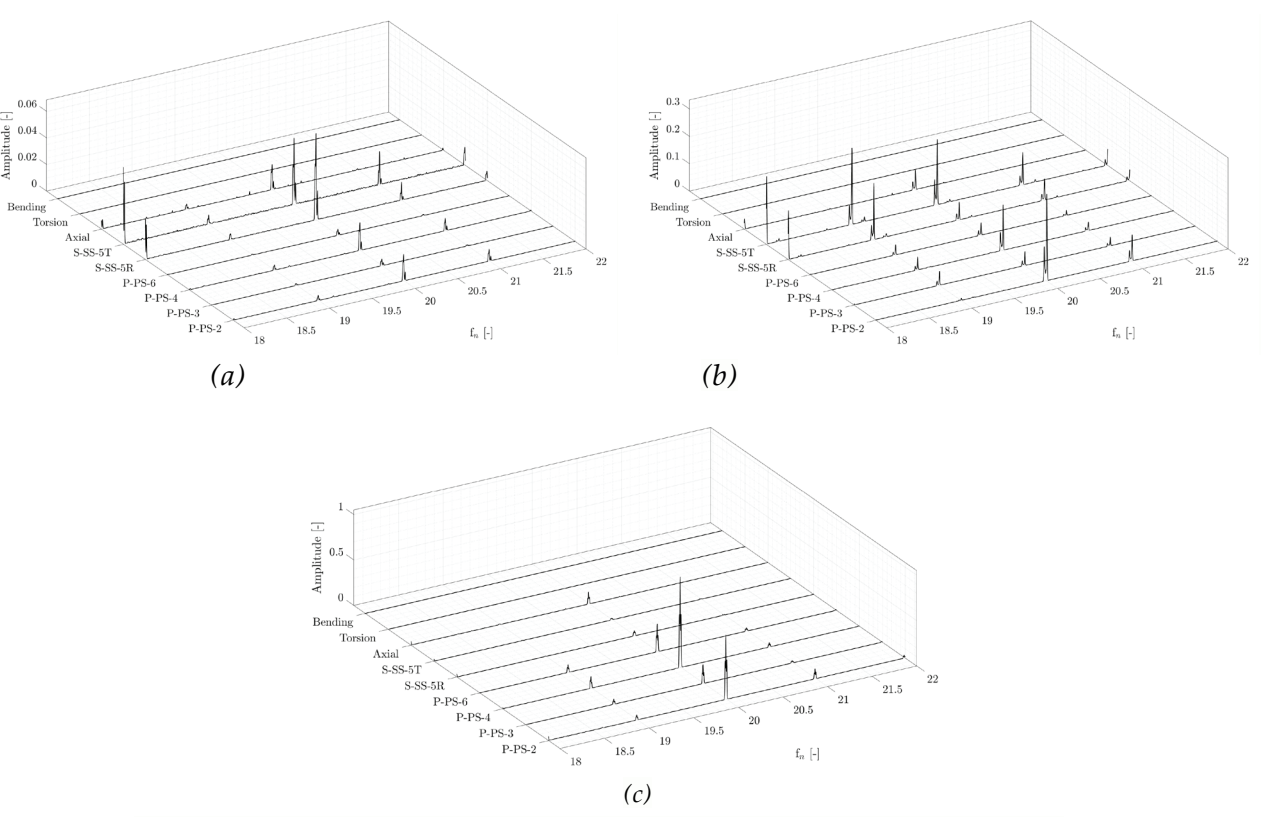


Figure 4.14: Waterfall plots of pressure and strain data obtained on the runner blade and shaft at high-frequency region; (a)OP1, (b) OP3, and (c) OP5.



The fatigue analysis was performed based on the relative method defined in section 3.4. Rainflow cycle counting was used and a sensitivity analysis was performed to investigate the effect of the number of bins on the relative damage factor. Figure 4.15 shows the relative damage factor variation for different operating conditions considering 10, 15, and 25 bins based on the strain gauge data obtained close to the blade hub. It is observed that the effect of the number of bins on the relative damage factor is negligible.

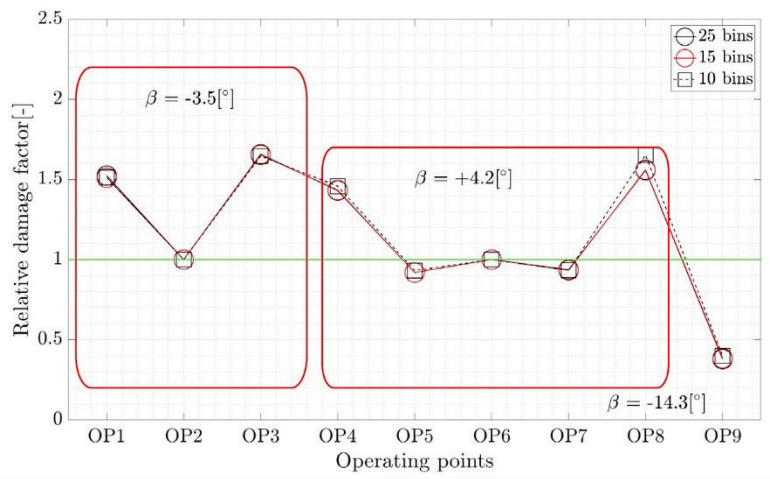


Figure 4.15: Relative damage factor for different operating points considering 10, 15, and 25 bins based on the strain gauge data obtained close to the blade hub in the radial direction (S-SS-5R)

The relative damage factor is plotted for different operating conditions in Figure 4.16. Strain gauges installed close to the blade hub and the trailing edge were used. Operating conditions consisted of seven steady-state operating points, start, speed-no-load, excitation, and stop. The results show that steady- state operating points away from the BEP can result in a high relative damage factor reaching 1.5. Interestingly, the relative damage factor of below one is observed for the low-load operating point (OP11), start, speed-no-load, excitation, and stop.

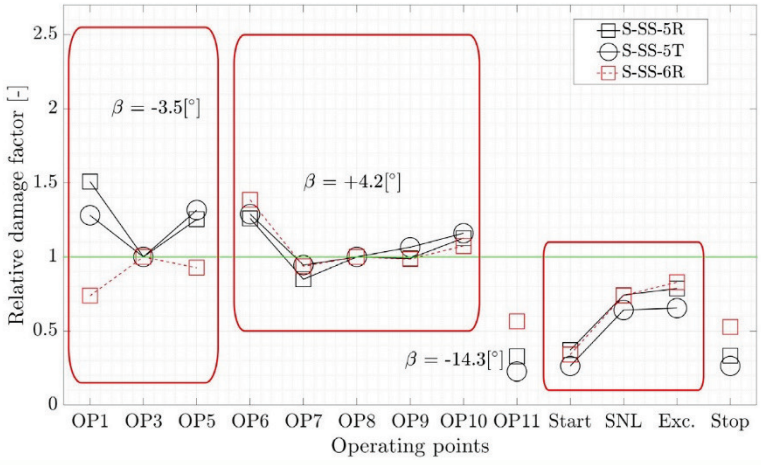


Figure 4.16: Relative damage factor for different operating points based on the strain gauge data obtained close to the blade hub and trailing edge.



The fluctuating component of the strain on the runner blades is an important parameter to investigate the fatigue life. The normalized peak-to-peak values of eight strain gauges are presented in Figure 4.17. The strain peak-to-peak values were normalized using the average value of each strain data during the last phase of the operation (steady-state operation, t_4). t_0 , t_1 , t_2 , t_3 , and t_4 corresponds to start-up, speed-no-load, excitation phase, load increase, and steady-state-operation. The results of strain gauges close to the blade hub (S-SS-5R and S-SS-5T) show that strain peak-to-peak values during start-up, speed-no-load, and excitation is less than steady-state operation (t_4). This could explain the relative damage factor results.

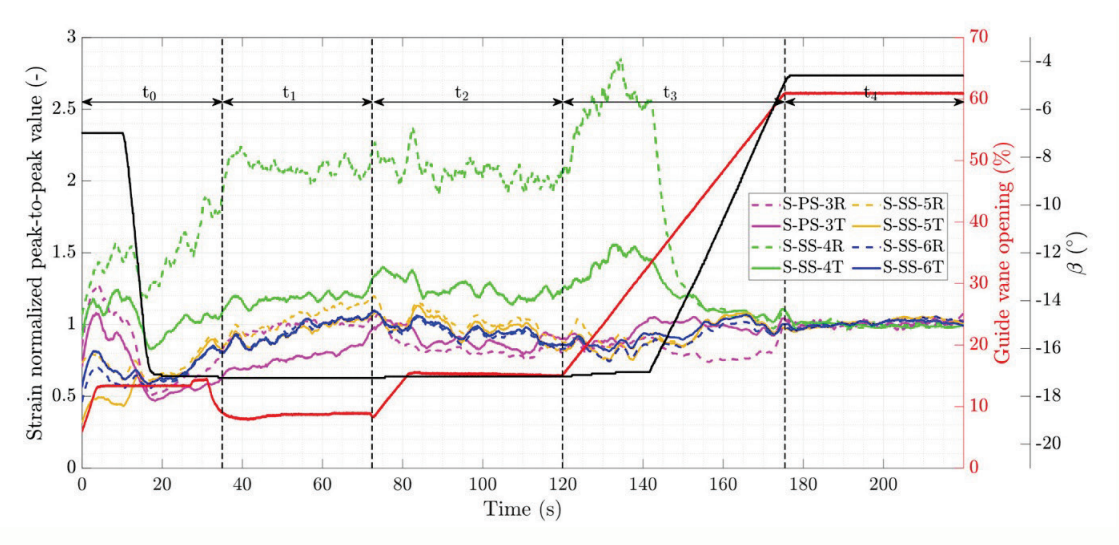


Figure 4.17: Normalized peak-to-peak value of strain fluctuations on the runner blade during the turbine start-up operation; red line: guide vane opening; black line: runner blade angle; vertical black dashed lines indicate the different stages of the start-up operation. (reproduced from [25]).



5 Conclusion

A successful measurement campaign was performed on the Porjus U9 Kaplan prototype turbine covering several operating conditions. The results showed that, for any propeller curve of a Kaplan turbine, the guide vane opening corresponding to the minimum pressure and strain fluctuation on the runner blade can also be obtained by the axial, torsion, and bending measurement on the shaft. Additionally, it was observed that torsion measurement on the shaft could be an indication for the index-test in Kaplan turbines. Spectral analysis of data obtained on the runner blade and shaft showed that a signature of every phenomenon observed in the turbine chamber can also be detected in the data on the shaft. For example, rotating vortex rope, runner frequency, and guide vane passing frequency were detected in both data obtained on the runner blade and shaft. Therefore, operating points with the possibility of high-stress fluctuation on the runner blade can be avoided by performing measurements on the shaft. The fatigue analysis showed that steady-state operating points away from the BEP can result in a high relative damage factor reaching 1.5. However, the low-load operating point, startup, speed-no-load, excitation, and stop has a lower relative damage factor (<1).



6 References

- 1. Murdock, H.E., Gibb, D., André, T., Appavou, F., Brown, A., Epp, B., Kondev, B., McCrone, A., Musolino, E. and Ranalder, L., 2019. *Renewables* 2019 Global Status Report.
- 2. Swedish Energy Agency, 2019. *Energy in Sweden* 2019 *An overview*. Eskilstuna, Sweden:www.energimyndigheten.se.
- 3. Escudier, M., 1987. *Confined vortices in flow machinery*. Annual Review of Fluid Mechanics, 19(1), pp. 27-52.
- 4. Trivedi, C., Cervantes, M.J., Gandhi, B.K. and Dahlhaug, O.G., 2013. Experimental and numerical studies for a high head Francis turbine at several operating points. Journal of FluidsEngineering, 135(11), pp. 111102.
- 5. Amiri, K., Cervantes, M.J. and Mulu, B., 2015. *Experimental investigation of the hydraulic loadson the runner of a Kaplan turbine model and the corresponding prototype*. Journal of Hydraulic Research, 53(4), pp. 452-465.
- 6. Amiri, K., Mulu, B. and Cervantes, M.J., 2016. Experimental Investigation of the Interblade Flow in a Kaplan Runner at Several Operating Points Using Laser Doppler Anemometry. Journal of FluidsEngineering, 138(2), pp. 021106.
- 7. Trivedi, C., Gandhi, B. and Michel, C.J., 2013. Effect of transients on Francis turbine runner life:a review. Journal of Hydraulic Research, 51(2), pp. 121-132.
- 8. Trivedi, C., 2017. *A review on fluid structure interaction in hydraulic turbines: A focus onhydrodynamic damping*. Engineering Failure Analysis, 77, pp. 1-22.
- 9. Trivedi, C. and Cervantes, M.J., 2017. Fluid-structure interactions in Francis turbines: Aperspective review. Renewable and Sustainable Energy Reviews, 68, pp. 87-101.
- 10. Huth, H., 2005. *Fatigue design of hydraulic turbine runners*, Norwegian University of Science and Technology, Ph.D. thesis.
- 11. Coutu, A., Gagnon, M. and Monette, C., *Life assessment of francis runners using strain gage sitemeasurements*, Waterpower XV, July 23-27.
- 12. Antonsen, Ø, 2007. *Unsteady flow in wicket gate and runner with focus on static and dynamicload on runner*, Norwegian University of Science and Technology, Ph.D. thesis.
- 13. Presas, A., Luo, Y., Wang, Z. and Guo, B., 2019. Fatigue life estimation of Francis turbines based on experimental strain measurements: Review of the actual data and future trends. Renewableand Sustainable Energy Reviews,



- 102(March 2019), pp. 96-110.
- 14. Simmons, G.F., 2013. *Journal bearing design, lubrication and operation for enhanced performance*, Lulea university of technology, Ph.D. thesis.
- 15. Pino, G., Ribas, J.R. and Guimarães, L.F., 2018. Bearing diagnostics of hydro power plants usingwavelet packet transform and a hidden Markov model with orbit curves. Shock and Vibration, 2018.
- Valentín, D., Presas, A., Valero, C., Egusquiza, M. and Egusquiza, E., 2019. Detection of Hydraulic Phenomena in Francis Turbines with Different Sensors. Sensors, 19(18), pp. 4053.
- 17. Trivedi, C., Gogstad, P.J. and Dahlhaug, O.G., 2018. *Investigation of the unsteady pressure pulsations in the prototype Francis turbines—Part 1: Steady state operating conditions*. Mechanical Systems and Signal Processing, 108, pp. 188-202.
- 18. Trivedi, C., Gogstad, P.J. and Dahlhaug, O.G., 2017. *Investigation of the unsteady pressure pulsations in the prototype Francis turbines during load variation and startup*. Journal of Renewableand Sustainable Energy, 9(6), pp. 064502.
- 19. Wang, W., Chen, Q. and Yan, D., 2018. *Hydraulic stability analysis of a large prototype Francisturbine based on field test.* Journal of Fluids Engineering, 140(11), pp. 114501.
- 20. Gagnon, M., Jobidon, N., Lawrence, M. and Larouche, D., Optimization of turbine startup: Someexperimental results from a propeller runner, The 27th IAHR Symposium on Hydraulic Machinery and Systems, 22-26 September 2014, IOP Publishing, pp. 032022.
- 21. Gagnon, M., Tahan, S.A., Bocher, P. and Thibault, D., *Impact of startup scheme on Francisrunner life expectancy*, 25th IAHR Symposium on Hydraulic Machinery and Systems, 20–24 September 2010, IOP Publishing, pp. 012107.
- 22. Jansson, I., 2013. Vibrant Bodies of Swirling Flow: On the limits of mechanical powertransformation, Lulea university of technology, Ph.D. thesis.
- 23. Soltani Dehkharqani, A., 2020. An Experimental Investigation of a Prototype Kaplan Turbine and Numerical Analysis of Fluid Added Parameters on the Corresponding Model Turbine Runner, Luleå University of Technology, Ph.D. thesis.
- 24. Amiri, K., 2016. Experimental investigation of a Kaplan runner under steadystate and transientoperations, Lulea university of technology, Ph.D. thesis.
- 25. Soltani Dehkharqani, A., Engström, F., Aidanpää, J. and Cervantes, M.J., 2019. Experimental Investigation of a 10 MW Prototype Kaplan Turbine during Start-Up Operation. Energies, 12(23), pp. 4582.



LOADS ON KAPLAN RUNNER DURING STEADY OPERATIONS

Sol och vind ställer nya krav på vattenkraften. Instabila flöden med variationer i tryck och belastning ger ökat slitage på turbinerna.

I det här projektet har ny kunskap tagits fram för att bland annat minska risken för haveri av turbinerna och att minska de i många fall höga kostnaderna för reparationer och produktionsbortfall.

För att bedöma och förutsäga flödesförhållanden och belastningar på löphjulet för en Kaplanturbin har en experimentell metodik utvecklats för att koppla mätningar på axeln till mätningar på turbinebladen. Turbulenta flöden har analyserats och nya numeriska tekniker, metoder och modeller för framtiden har utvecklats.

Energiforsk is the Swedish Energy Research Centre – an industrially owned body dedicated to meeting the common energy challenges faced by industries, authorities and society. Our vision is to be hub of Swedish energy research and our mission is to make the world of energy smarter!

